JOURNAL OF AIRCRAFT
Vol. 44, No. 3, May–June 2007

Predicting Maximum Lift Coefficient for Twisted Wings Using Computational Fluid Dynamics

N. R. Alley,* W. F. Phillips,† and R. E. Spall‡
Utah State University, Logan, Utah 84322-4130

DOI: 10.2514/1.25643

A method is presented that allows one to predict the maximum lift coefficient for a finite wing from knowledge of wing geometry and maximum airfoil section lift coefficient. This approach applies to wings of arbitrary planform and includes the effects of twist and sweep. The method uses a correlation obtained from grid-resolved computational fluid dynamics solutions for 25 different wing geometries. These wings had aspect ratios ranging from 4 to 20, taper ratios from 0.5 to 1.0, quarter-chord sweep angles from 0 to 30 deg, and linear geometric washout ranging from 0 to 8 deg. For this range of parameters, the ratio of maximum wing lift coefficient to maximum airfoil section lift coefficient varied from about 0.70 to 0.98, with high-aspect-ratio tapered wings producing the highest values and low-aspect-ratio wings with washout and sweep producing the lowest values.

Nomenclature

C_L	=	wing lift coefficient
$\tilde{C}_L$	=	local airfoil section lift coefficient
$C_{L_{\max}}$	=	maximum wing lift coefficient
$\tilde{C}_{L_{\max}}$	=	maximum airfoil section lift coefficient
$C_{L,\alpha}$	=	wing lift slope
$\tilde{C}_{L,\alpha}$	=	airfoil section lift slope
i	=	spanwise grid index integer
j	=	streamwise grid index integer
k	=	radial grid index integer
M	=	Mach number
R	=	Reynolds number
R_A	=	wing aspect ratio
R_T	=	wing taper ratio
y^+	=	shear Reynolds number for the grid layer next to the airfoil or wing surface
κ_{Ls}	=	stall factor in the relation for maximum lift coefficient
$\kappa_{L\Lambda}$	=	sweep factor in the relation for maximum lift coefficient
$\kappa_{L\Omega}$	=	twist factor in the relation for maximum lift coefficient
Λ	=	quarter-chord sweep angle
Ω	=	total wing twist angle from the root to the wingtip

Introduction

MANY facets of aircraft design and performance prediction require knowledge of the maximum lift coefficient that can be developed by a lifting wing before stall. Generally, the local section lift coefficient is not constant across the span of a wing. Thus, the maximum lift coefficient that can be generated by a wing is typically less than the maximum section lift coefficient for the airfoil section used to form the wing. For these reasons there is considerable interest in the determination of the maximum lift coefficient for finite wings [1–7].

One method commonly used to help control the stall characteristics of a wing involves the introduction of wing twist. For untwisted wings with taper and/or sweep, the wing section that supports the maximum section lift coefficient is located outboard from the wing root. This can interfere with roll control during stall recovery and give the aircraft poor handling characteristics. Washout is commonly added to such wings to alleviate this problem. Furthermore, with proper implementation, wing twist can be used to reduce drag [8–10] or increase the total lift that can be developed on a wing before stall [11]. Thus, it is important to be able to predict the effects of wing twist on maximum lift coefficient.

For a finite wing of arbitrary planform and twist, Prandtl's lifting-line theory [12,13] can be used to predict the wing lift coefficient that is developed at the onset of airfoil section stall [11]. This is accomplished by integrating the predicted section lift distribution over the span of the wing, with the root angle of attack set to that for which the maximum wing section lift coefficient is equal to the maximum possible airfoil section lift coefficient. Such lifting-line analysis results in the relation

$$\frac{C_L}{\tilde{C}_{L_{\max}}} = \left(\frac{C_L}{\tilde{C}_{L_{\max}}}\right)_{\substack{\Omega=0\\ \Lambda=0}} \kappa_{L\Lambda}\left(1 - \kappa_{L\Omega}\frac{C_{L,\alpha}\Omega}{\tilde{C}_{L_{\max}}}\right) \tag{1}$$

In this relation, twist is treated as positive at outboard sections of the wing having a lower aerodynamic angle of attack than the root and negative at sections with a higher aerodynamic angle of attack than the root (i.e., washout is defined to be positive twist). The first term on the right-hand side of Eq. (1) is the ratio of the total wing lift coefficient to the maximum section lift coefficient for a wing having the same planform but without twist or sweep. This ratio can be determined as a function of wing planform from results presented by Phillips and Alley [11]. The sweep factor $\kappa_{L\Lambda}$ and the twist factor $\kappa_{L\Omega}$ can also be evaluated from knowledge of the wing geometry using results presented in [11].

Using the maximum airfoil section lift coefficient in Eq. (1) gives an estimate for the wing lift coefficient at the onset of airfoil section stall. At higher angles of attack, separated flow will exist over some sections of the wing and drag will be substantially increased. However, the lift coefficient predicted from Eq. (1) is not exactly the maximum wing lift coefficient. Viscous interactions between adjacent sections of the wing can initiate flow separation at slightly lower angles of attack than predicted by Eq. (1). Furthermore, as the angle of attack is increased somewhat beyond that which produces the onset of airfoil section stall, the section lift coefficient on the stalled section of the wing will decrease. However, the section lift coefficient on the unstalled sections of the wing will continue to

Presented as Paper 0898 at the 45th AIAA Aerospace Sciences Meeting and Exhibit, Reno, NV, 8–11 January 2007; received 5 June 2006; revision received 15 September 2006; accepted for publication 22 September 2006.

*Graduate Student, Mechanical and Aerospace Engineering Department, 4130 Old Main Hill. Student Member AIAA.
†Professor, Mechanical and Aerospace Engineering Department, 4130 Old Main Hill. Member AIAA.
‡Professor, Mechanical and Aerospace Engineering Department, 4130 Old Main Hill.

increase with angle of attack until the maximum section lift coefficient is reached on these sections as well. Thus, the maximum wing lift coefficient could differ slightly from that predicted by Eq. (1). To account for these effects, results predicted from Eq. (1) could be modified by including a stall correction factor,

$$\frac{C_L}{\tilde{C}_{L_{\max}}} = \left(\frac{C_L}{\tilde{C}_{L_{\max}}}\right)_{\substack{\Omega=0\\ \Lambda=0}} \kappa_{Ls}\kappa_{L\Lambda}\left(1 - \kappa_{L\Omega}\frac{C_{L,\alpha}\Omega}{\tilde{C}_{L_{\max}}}\right) \tag{2}$$

The purpose of the research investigation reported herein was to use computational fluid dynamics (CFD) to develop an algebraic correlation for the stall factor κ_{Ls} as a function of appropriate geometric parameters for wings with linear taper and linear twist.

Computational Methodology

Because Eq. (2) expresses the maximum wing lift coefficient in terms of the maximum airfoil section lift coefficient, developing a correlation for κ_{Ls} requires knowledge of the maximum 2-D airfoil lift coefficient as well as the maximum 3-D wing lift coefficient, both evaluated for the same Reynolds and Mach numbers. Such results could be obtained from either experimental data or computational methods. For the results presented here, CFD solutions were used.

The NACA 0012 airfoil was chosen as the base airfoil section for the 2-D and 3-D computations. All calculations were performed using version 6 of the computational fluid dynamics code CFL3D [14]. This is a structured-grid, multizone code that solves the three-dimensional, time-dependent, Reynolds-averaged, Navier–Stokes equations using an upwind finite-volume formulation. The code uses a third-order upwind biased interpolation scheme for the convective and pressure terms. Local time stepping, mesh sequencing, and low-Mach-number preconditioning were also used. The Spalart–Allmaras turbulence model [15] was used for all computations and all results were obtained for a freestream Mach number of 0.25 and a freestream Reynolds number of 3.0×10^6.

For predicting the 3-D wing lift coefficients used in the present study, all computations were performed using C–O grids generated about one semispan of a finite wing. Inflow/outflow boundary conditions were specified on the far-field planes and symmetry conditions were used along the bounding plane at the wing root. No-slip boundary conditions were specified on the wing surface. To ensure that the 3-D solutions for maximum wing lift coefficient were grid-resolved, initial computations were made starting with a grid previously demonstrated to give grid-resolved solutions to the Euler equations [10]. This Euler grid was chosen as a starting point to ensure that the wingtip vortex and resulting downwash were adequately resolved. For this C–O grid, nodes were distributed over a computational domain that extended 10 chord lengths from the wing in all directions. Nodes were clustered in the chordwise direction near the leading and trailing edges of the wing and in the spanwise direction near the wingtip. Nodes were also clustered in the wake region aft of the wingtip, to provide improved resolution of the wingtip vortex. For the initial viscous computations, the Euler grid was refined in the region close to the wing so that the normal grid spacing at the wing surface was reduced to 1.0×10^{-5} chord lengths. The refinement was carried out by increasing the number of radial nodes and adjusting the radial growth factor in the region close to the wing, so that first-order grid smoothness was retained as the normal grid spacing in the boundary layer was reduced. This initial grid was then further refined iteratively, using a similar procedure, until no significant change was observed in the solution for the angle of attack corresponding to the maximum wing lift coefficient. In all cases, the average y^+ value for the surface boundary elements of the final grid was on the order of 1. Figures 1–5 show several sections of a typical grid developed in this manner. To aid in visibility, only every fourth node in all three directions is shown in Figs. 1–3 and only the odd nodes in all three directions are shown in Figs. 4 and 5. This C–O grid has 121 spanwise sections with 385 nodes spaced around the circumference of each wing section. An additional 160 streamwise nodes are included in the trailing wake for each spanwise section. A total of 233 radial layers are used to create this $121 \times 545 \times 233$ C–O grid containing 15,365,185 nodes.

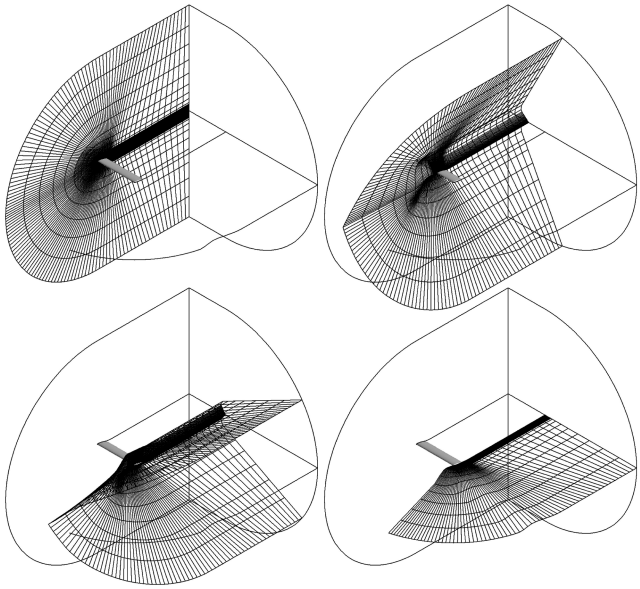

Fig. 1 Constant-*i* planes for a typical C–O grid.

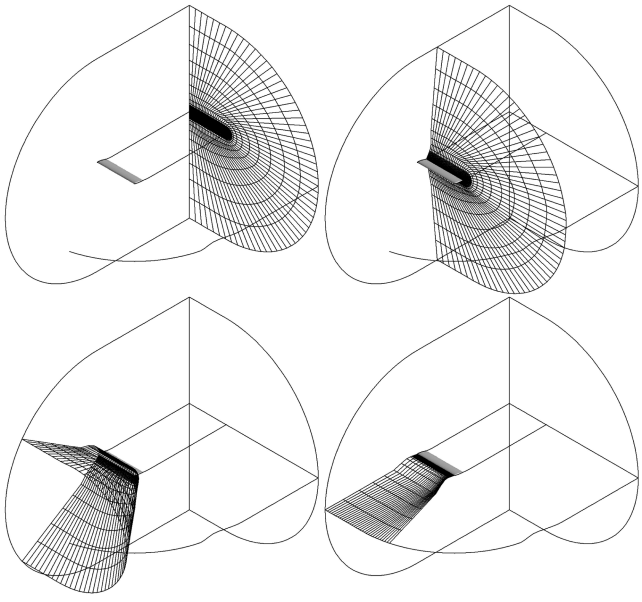

Fig. 2 Constant-*j* planes for a typical C–O grid.

To evaluate grid resolution and for use in mesh sequencing, a family of four similar grids was generated from the initial refined grid, which was developed as described earlier and is hereafter referred to as the *fine grid*. To create the four-grid family, a *medium grid* was next generated by removing every other point in each coordinate direction from the fine grid. A *coarse grid* was then generated by similarly removing every other point from the medium grid. Finally, an *extra-fine grid* was generated by globally refining the coarse grid by a factor of 6 in each coordinate direction. Typical results of a 3-D grid-convergence study obtained from this family of grids are shown in Fig. 6. From these results, the lift coefficient solutions obtained from the fine grid and displayed as small filled circles are shown to be grid-resolved for those angles of attack less than or equal to that which produces the maximum wing lift coefficient. For the results obtained with this C–O grid at the angles of attack shown in Fig. 6, the average y^+ values for the surface boundary elements ranged from 1.12 to 1.22. The y^+ values given in Fig. 6 are the average values for the angle of attack that produced the maximum wing lift coefficient.

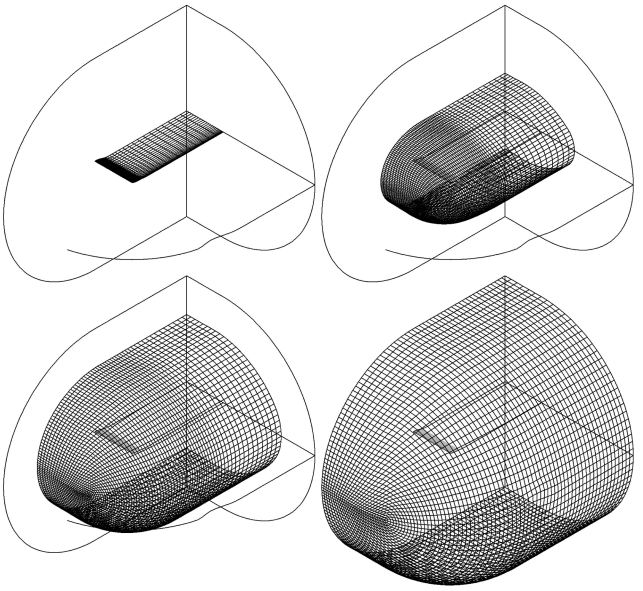

Fig. 3 Constant-*k* planes for a typical C–O grid.

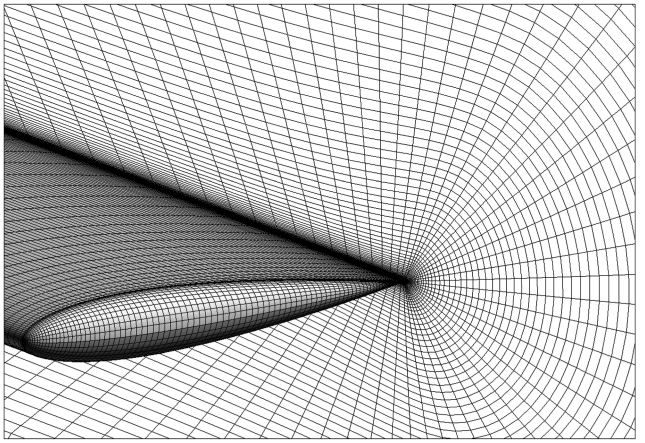

Fig. 4 Constant-*j* planes at the trailing edge of the wingtip and constant-*k* plane on the wing surface.

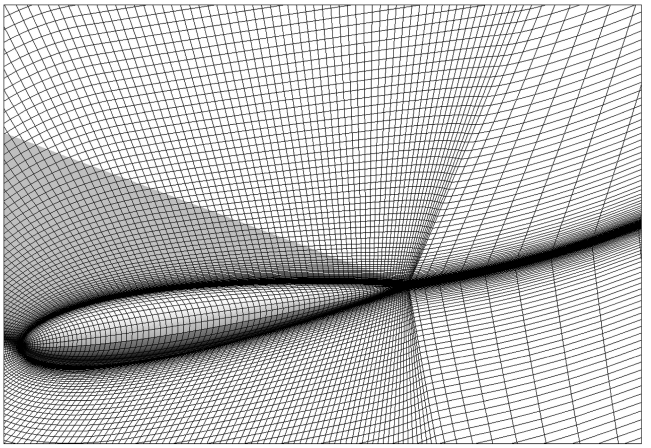

Fig. 5 Constant-*i* plane at the base of the end cap and constant-*k* plane on the end cap surface.

In addition to the grid-convergence studies discussed earlier, which were performed on a fixed computational domain extending 10 chord lengths from the wing in all directions, a larger computational domain was also used for a subset of the 3-D calculations. Results obtained for this larger computational domain,

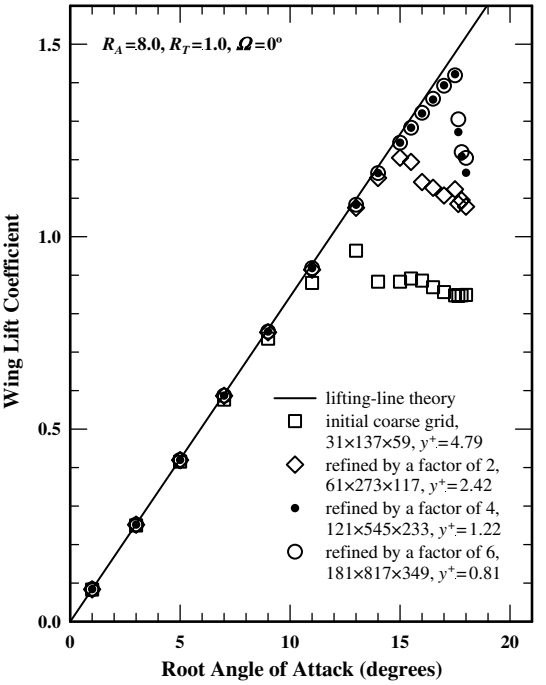

Fig. 6 Grid-convergence study for a rectangular wing operating at a freestream Reynolds number of 3.0×10^6 and a freestream Mach number of 0.25.

which extended 20 chord lengths from the wing, revealed changes in the lift coefficient of less than 1% when compared with results obtained from the 10-chord domain. This comparison for a typical wing is shown in Fig. 7. Based on these and other similar results, the 10-chord domain was deemed sufficient for the remainder of the computations.

Determining the ratio of maximum lift coefficients expressed in Eq. (2) requires evaluating the maximum 2-D airfoil section lift coefficient as well as the maximum 3-D wing lift coefficient. To ensure that the 2-D solutions were also grid-resolved, grid-

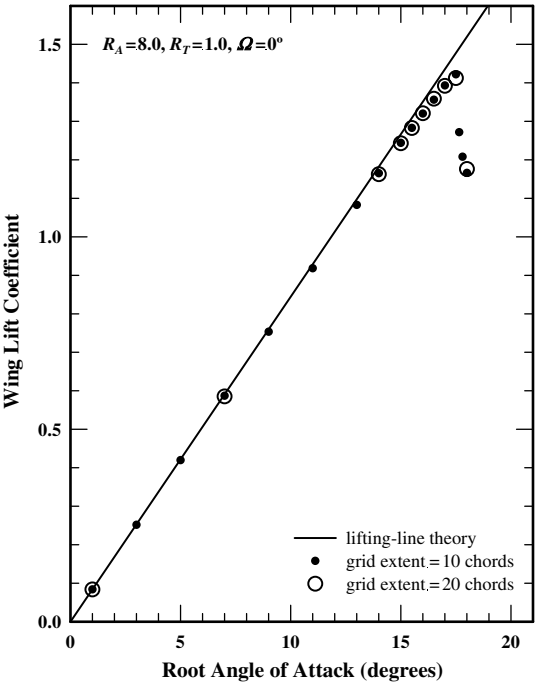

Fig. 7 Effect of computational domain size on grid resolution for a rectangular wing operating at a freestream Reynolds number of 3.0×10^6 and a freestream Mach number of 0.25.

convergence studies similar to those described for the 3-D computations were carried out for the 2-D computations as well.

It is essential that the 3-D wing computations are carried out for the same Reynolds and Mach numbers as used for the 2-D airfoil computations. For the case of a rectangular wing this is rather straightforward. However, for a tapered wing the section Reynolds number is not constant across the wingspan. This gives rise to an important question as to what characteristic length should be used to define the Reynolds number associated with predicting the maximum lift coefficient for a tapered wing.

Two different chord lengths are commonly used as the streamwise characteristic length for a finite wing. The simplest of these is the arithmetic mean chord, i.e., the wing planform area divided by the wingspan. The other is what is commonly called the aerodynamic mean chord, which is defined to be the chord length at the spanwise coordinate that corresponds to the aerodynamic center of the wing semispan. Neither of these two definitions provides a particularly suitable characteristic length for defining the Reynolds number associated with wing stall. A more appropriate characteristic length for this purpose is the chord length at the spanwise coordinate that supports the maximum airfoil section lift coefficient.

The spanwise position of the maximum section lift coefficient at the onset of airfoil section stall depends on wing taper, twist, and sweep. For an untwisted rectangular wing with no sweep, the onset of airfoil section stall occurs at the wing root. As wing taper ratio is decreased from 1.0, the point of maximum section lift coefficient moves outboard from the root. Adding sweep to the wing also moves the point of maximum section lift coefficient outboard. On the other hand, adding washout to a wing with taper and/or sweep moves the point of maximum section lift coefficient inboard. Lifting-line theory can be used to predict the spanwise coordinate of the wing section that supports the maximum airfoil section lift coefficient [11].

For the computations used in the present study, the characteristic length specified for computing the Reynolds number was the chord length at the wing section that carries the maximum section lift coefficient, as predicted by lifting-line theory. For each wing considered, the root chord was adjusted as a function of taper, twist, and sweep so that all wings had the same chord length at the spanwise position of the maximum section lift coefficient. This same chord length was also used in the 2-D computations for the maximum airfoil section lift coefficient. Figure 8 shows typical grid-convergence results for a tapered wing with linear washout, as obtained using this method for defining the Reynolds number.

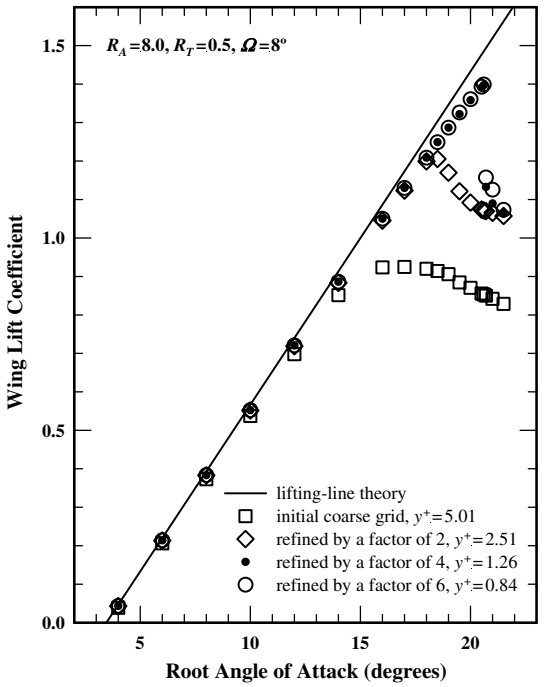

Fig. 8 Grid-convergence study for a tapered wing with 8 deg of linear washout operating at a freestream Reynolds number of 3.0×10^6 and a freestream Mach number of 0.25.

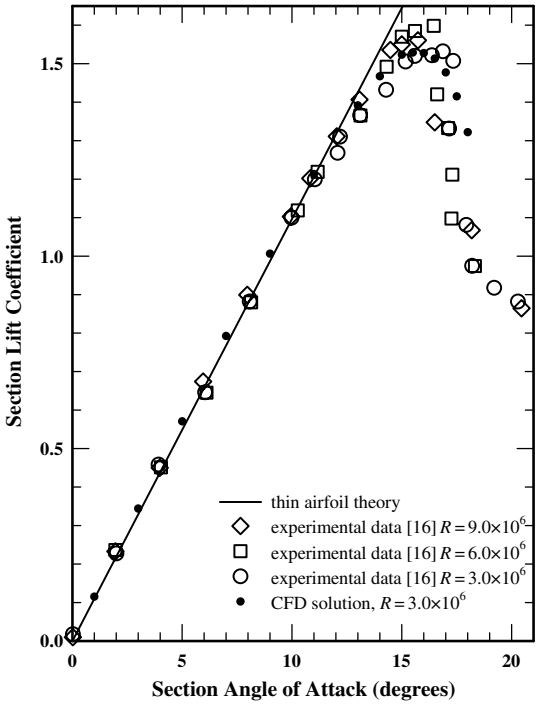

Fig. 9 Comparison between experimental data for a NACA 0012 airfoil section and two-dimensional CFD results obtained for the same airfoil operating at a freestream Reynolds number of 3.0×10^6 and a freestream Mach number of 0.25.

Results

Although the results shown in the preceding section indicate that grid-resolved CFD solutions have been obtained for the Reynolds-averaged Navier–Stokes equations combined with the Spalart–Allmaras turbulence model, this grid-convergence study gives no insight into the accuracy of the solutions. In Fig. 9 the 2-D solutions are compared with experimental data reported by Abbott and Von Doenhoff [16]. This figure is presented here only to show that the CFD results are reasonable for a Reynolds number of 3.0×10^6. In the present study, we made no attempt to evaluate the dependence of maximum wing lift coefficients on wing geometry for a broad range of Reynolds and Mach numbers. However, for this investigation we are interested only in evaluating the low-Mach-number ratio of a 3-D maximum wing lift coefficient to the corresponding 2-D maximum airfoil section lift coefficient. Because changes in the Reynolds number at low Mach numbers should affect the 2-D and 3-D lift coefficients in a similar manner, Reynolds number dependences should not greatly affect the ratio $C_{L_{\max}}/\tilde{C}_{L_{\max}}$, provided that the same Reynolds and Mach numbers are used for both computations. When compared with experimental data for airfoil sections of widely differing geometries [16], CFD results obtained using the Spalart–Allmaras turbulence model were found to predict the maximum section lift coefficient reasonably well for a Reynolds number of 3.0×10^6. At higher Reynolds numbers the agreement was not as good, in spite of the fact that the grids were refined to maintain grid resolution and keep the y^+ values on the order of 1. For this reason, and because higher Reynolds numbers require finer grids, the freestream Reynolds number was fixed at 3.0×10^6 for the computations used in the present study to evaluate κ_{Ls}.

To obtain some insight into the accuracy of the 3-D computations, Fig. 10 shows a comparison between grid-resolved CFD solutions and experimental data reported by Fitzpatrick and Schneider [5]. The wing used for this comparison had an aspect ratio of 6.0, a taper ratio of 0.5, a quarter-chord sweep of 3.18 deg, and 1.5 deg of linear washout. Both the CFD solutions and the experimental data were

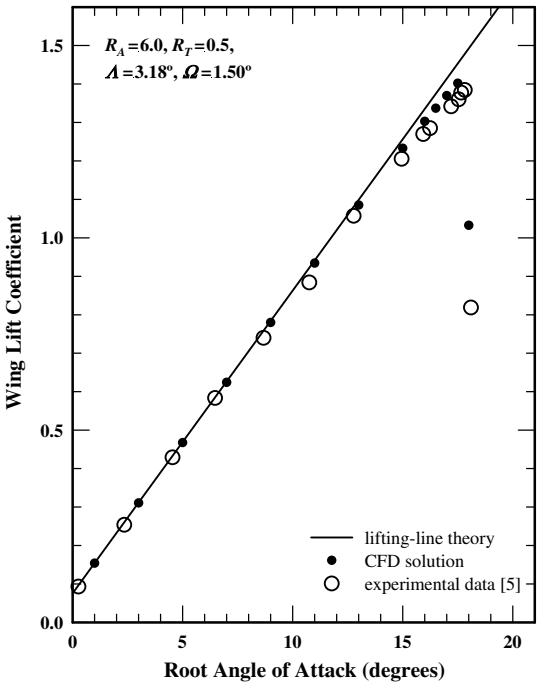

Fig. 10 Comparison between experimental data and CFD results for a tapered wing of NACA 64-210 airfoil section operating at a freestream Reynolds number of 3.15×10^6 and a freestream Mach number of 0.10.

obtained for a freestream Reynolds number of 3.15×10^6 and a freestream Mach number of 0.10. The lifting-line solution shown in Fig. 10 was obtained using an airfoil section lift slope predicted from 2-D grid-resolved CFD solutions for the NACA 64-210 airfoil.

For any particular wing geometry, the value of the stall factor κ_{Ls}, as defined in Eq. (2), can be estimated from 2-D and 3-D grid-resolved CFD solutions using the relation

$$\kappa_{Ls} \equiv \frac{C_{L_{\max}}/\tilde{C}_{L_{\max}}}{(C_L/\tilde{C}_{L_{\max}})_{\substack{\Omega=0\\ \Lambda=0}} \kappa_{L\Lambda}[1-\kappa_{L\Omega}(C_{L,\alpha}\Omega/\tilde{C}_{L_{\max}})]} \tag{3}$$

where the numerator on the right-hand side of Eq. (3) is evaluated from CFD computations and the denominator is evaluated from lifting-line theory. For a wing of arbitrary planform and twist, evaluating the denominator on the right-hand side of Eq. (3) from lifting-line theory requires knowledge of the airfoil section lift slope and the maximum airfoil section lift coefficient. The 2-D computational results were also used for this purpose.

In the present study, the maximum wing lift coefficient was determined from CFD solutions for 25 different wing geometries. These wings had aspect ratios ranging from 4 to 20, taper ratios from 0.5 to 1.0, quarter-chord sweep angles from 0 to 30 deg, and linear geometric washout ranging from 0 to 8 deg. For 24 of the 25 wings the NACA 0012 airfoil section was used. The remaining wing, which was that used to obtain the results shown in Fig. 10, had a NACA 64-210 airfoil section. For each of these 25 wings, the stall factor κ_{Ls} was evaluated from the CFD results using Eq. (3). The outcome revealed that the geometric parameters having the most significant effect on κ_{Ls} were the aspect ratio and wing twist.

Figure 11 shows all of the results obtained in the present study, plotted as a function of wing aspect ratio. The results obtained for only the untwisted wings can all be correlated closely with the linear relation

$$(\kappa_{Ls}-1)_{\Omega=0} = 0.0042R_A - 0.068 \tag{4}$$

This correlation is also displayed in Fig. 11 as the solid line. From this figure it is readily observed that the stall factors obtained for twisted wings do not correlate well with Eq. (4). Thus, we can conclude that wing twist also affects κ_{Ls} significantly.

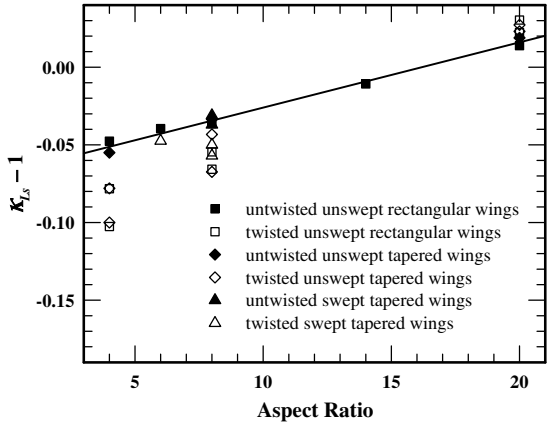

Fig. 11 Effect of wing aspect ratio on the stall factor as obtained from CFD solutions.

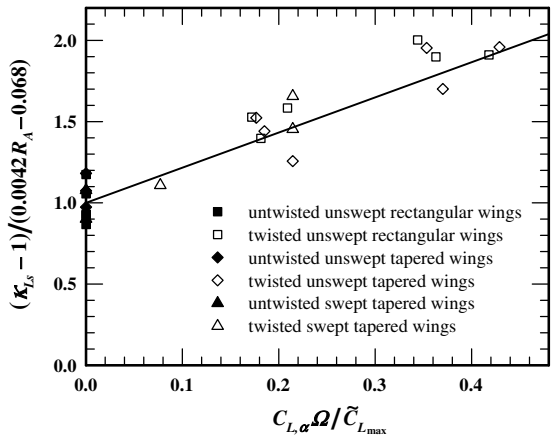

Fig. 12 Effect of wing twist on the stall factor as obtained from CFD solutions.

The variation of κ_{Ls} with wing twist is more easily visualized from Fig. 12. In this figure, $\kappa_{Ls}-1$ divided by the right-hand side of Eq. (4) is plotted as a function of dimensionless wing twist. The trend line shown in Fig. 12 is given by the relation

$$\frac{\kappa_{Ls}-1}{0.0042R_A-0.068} = 1 + 2.3\frac{C_{L,\alpha}\Omega}{\tilde{C}_{L_{\max}}} \tag{5}$$

Although the CFD results plotted in Fig. 12 are widely scattered about this linear correlation, no other significant trends in the computational results were observed. Furthermore, because the overall effect of wing twist on κ_{Ls} is only on the order of 5% or less, the scatter shown in Fig. 12 does not affect the accuracy of the final correlation as much as might be expected.

Rearranging Eq. (5) provides a simple algebraic correlation for the stall factor κ_{Ls}, which can be used in Eq. (2) to estimate the maximum lift coefficient for wings with linear taper and linear twist,

$$\kappa_{Ls} = 1 + (0.0042R_A - 0.068)(1 + 2.3C_{L,\alpha}\Omega/\tilde{C}_{L_{\max}}) \tag{6}$$

Figure 13 displays a comparison between this correlation and the grid-resolved CFD results obtained in the present study. In all cases the correlation agrees with the results obtained from the CFD computations to within about ± 1 percent. This is certainly well within the accuracy that can be expected for predicting flow separation using computational fluid dynamics.

When the correlation expressed in Eq. (6) is used to estimate the stall factor, and the result is used in Eq. (2) together with the lifting-line results presented by Phillips and Alley [11], the ratio of the maximum wing lift coefficient to the maximum airfoil section lift coefficient can be estimated from knowledge of the wing geometry.

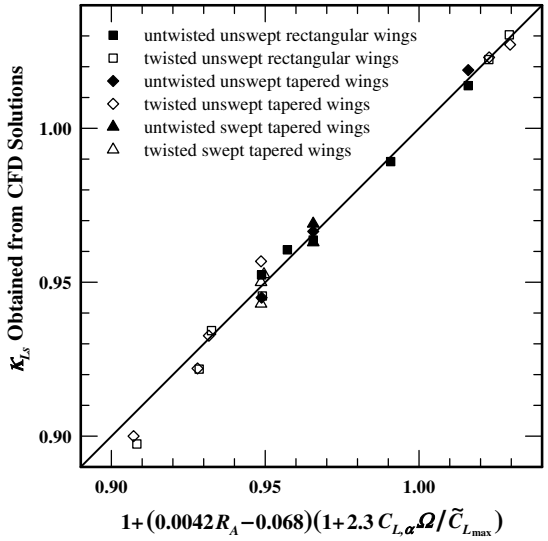

Fig. 13 Comparison between the stall factors obtained from CFD solutions and those obtained from the correlation given by Eq. (6).

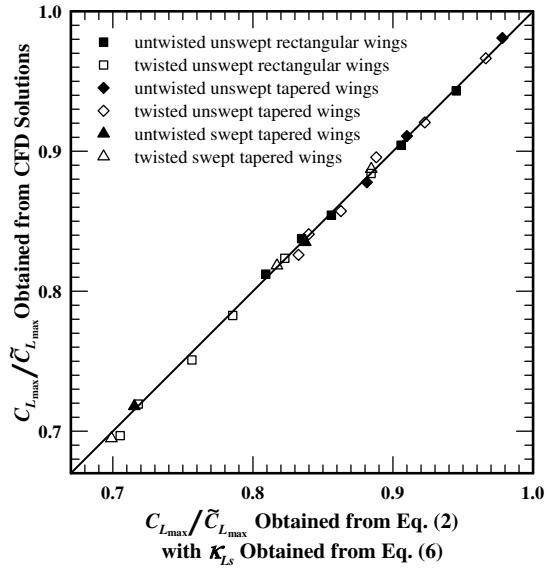

Fig. 14 Ratio of the maximum wing lift coefficient to the maximum airfoil section lift coefficient, as predicted from Eq. (2), compared with results predicted from CFD solutions in the present study.

Figure 14 shows a comparison between results obtained from Eq. (2) and the CFD results obtained in the present study. For the range of wing parameters investigated, the ratio $C_{L_{\max}}/\tilde{C}_{L_{\max}}$ varied from about 0.70 to 0.98, with high-aspect-ratio tapered wings producing the highest values. The lowest values of $C_{L_{\max}}/\tilde{C}_{L_{\max}}$ occurred for low-aspect-ratio wings with a high degree of washout and/or sweep.

From the results plotted in Fig. 13, it can be seen that the stall factor correction predicted from Eq. (6) is less than 10%. Thus, a reasonable first approximation for the maximum wing lift coefficient could be obtained directly from lifting-line theory, by neglecting the stall factor completely. Figure 15 shows a comparison between the CFD results obtained in the present study and such lifting-line results, obtained from Eq. (2) with $\kappa_{Ls} = 1.0$.

Conclusions

The correlation presented in Eq. (6) can be combined with results obtained from lifting-line theory to provide an improved relation for estimating the maximum wing lift coefficient from known wing geometry and airfoil section properties. Results predicted from this algebraic relation agree with the CFD results obtained in the present

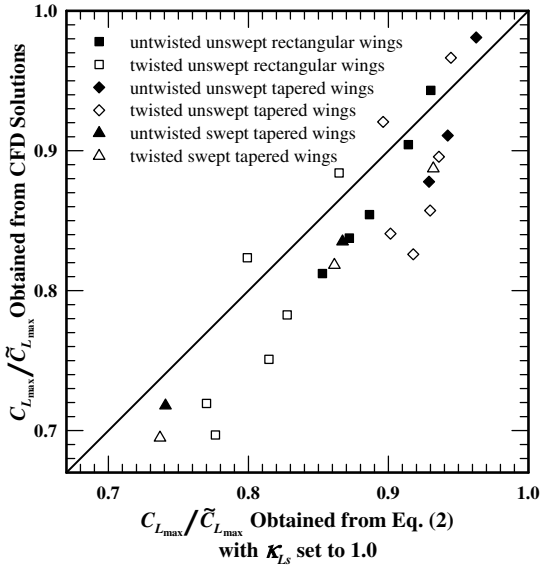

Fig. 15 Ratio of the maximum wing lift coefficient to the maximum airfoil section lift coefficient, as predicted from Eq. (2) with the stall factor set to 1.0, compared with results predicted from CFD solutions in the present study.

study to within ±1 percent. As might be expected, wing aspect ratio has the greatest effect on the ratio $C_{L_{\max}}/\tilde{C}_{L_{\max}}$, with this ratio approaching unity for very high-aspect-ratio wings. With all other things being equal, tapered wings exhibit a higher ratio of maximum wing lift coefficient to maximum airfoil section lift coefficient than do rectangular wings. On the other hand, both washout and sweep tend to reduce the maximum lift coefficient that can be developed on a finite wing with a given spanwise chord-length distribution and airfoil section properties.

Using lifting-line theory to estimate maximum wing lift coefficient provides a tremendous computational savings compared with the requirements for obtaining grid-resolved CFD solutions. In the present study, we were unable to develop a structured C–O grid with less than 15 million nodes per semispan, which would produce grid-resolved CFD solutions at a Reynolds number of 3.0×10^6 and the angle of attack that resulted in the maximum wing lift coefficient. For lower angles of attack, much coarser grids were found to give grid-resolved solutions. At post-stall angles of attack or higher Reynolds numbers, even finer grids were required.

References

[1] Silverstein, A., Katzoff, S., and Hootman, J. A., "Comparative Flight and Full-Scale Wind-Tunnel Measurements of the Maximum Lift of an Airplane," NACA TR-618, Feb. 1938.

[2] Spreiter, J. R., and Steffen, P. J., "Effects of Mach and Reynolds Numbers on Maximum Lift Coefficient," NACA TN-1044, March 1946.

[3] Sweberg, H. H., and Dingeldein, R. C., "Summary of Measurements in Langley Full-Scale Tunnel of Maximum Lift Coefficient and Stalling Characteristics of Airplanes," NACA TR-829, March 1947.

[4] Furlong, G. C., and Fitzpatrick, J. E., "Effects of Mach Number and Reynolds Number on the Maximum Lift Coefficient of a Wing of NACA 230-Series Airfoil Section," NACA TN-1299, May 1947.

[5] Fitzpatrick, J. E., and Schneider, W. C., "Effects of Mach Number Variation between 0.07 and 0.34 and Reynolds Number Variation Between 0.97×10^6 and 8.10×10^6 on the Maximum Lift Coefficient of a Wing of NACA 64-210 Airfoil Section," NACA TN-2753, Aug. 1952.

[6] Valarezo, W. O., and Chin, V. D., "Method for the Prediction of Wing Maximum Lift," *Journal of Aircraft*, Vol. 31, No. 1, 1994, pp. 103–109.

[7] Patel, M. P., Sowle, Z. H., Corke, T. C., and He, C., "Autonomous Sensing and Control of Wing Stall Using a Smart Plasma Slat," AIAA Paper 2006-1207, Jan. 2006.

[8] Phillips, W. F., "Lifting-Line Analysis for Twisted Wings and Washout-Optimized Wings," *Journal of Aircraft*, Vol. 41, No. 1, 2004,

pp. 128–136.
[9] Phillips, W. F., Alley, N. R., and Goodrich, W. D., "Lifting-Line Analysis of Roll Control and Variable Twist," *Journal of Aircraft*, Vol. 41, No. 5, 2004, pp. 1169–1176.
[10] Phillips, W. F., Fugal, S. R., and Spall, R. E., "Minimizing Induced Drag with Wing Twist, Computational-Fluid-Dynamics Validation," *Journal of Aircraft*, Vol. 43, No. 2, 2006, pp. 437–444.
[11] Phillips, W. F., and Alley, N. R., "Predicting Maximum Lift Coefficient for Twisted Wings Using Lifting-Line Theory," *Journal of Aircraft* (to be published).
[12] Prandtl, L., "Tragflügel Theorie," *Nachricten von der Gesellschaft der Wissenschaften zu Göttingen*, Geschäeftliche Mitteilungen, Klasse, Germany, 1918, pp. 451–477.
[13] Prandtl, L., "Applications of Modern Hydrodynamics to Aeronautics," NACA TR-116, June 1921.
[14] Krist, S. L., Biedron, R. T., and Rumsey, C. L., "CFL3D Users Manual (Version 5)," NASA TM-1998-208444, June 1998.
[15] Spalart, P., and Allmaras, S., "A One-Equation Turbulence Model for Aerodynamic Flows," AIAA Paper 1992-0439, Jan. 1992.
[16] Abbott, I. H., and Von Doenhoff, A. E., "Aerodynamic Characteristics of Wing Sections," *Theory of Wing Sections*, Dover, New York, 1949, pp. 449–687.